Conf-910878--1

UCRL- JC-108161
PREPRINT

Impact of the Ice Phase on a Mesoscale Convective System: Implications of Cloud Parameterization and Cloud Radiative Properties

Hung-Neng S. Chin, Michael M. Bradley,
Charles R. Molenkamp, Keith E. Grant
and Catherine Chuang

Symposium on "Aerosol-Cloud-Climate Interactions"
XX General Assembly IUGG
Vienna, Austria
13-20 August 1991

August 1991

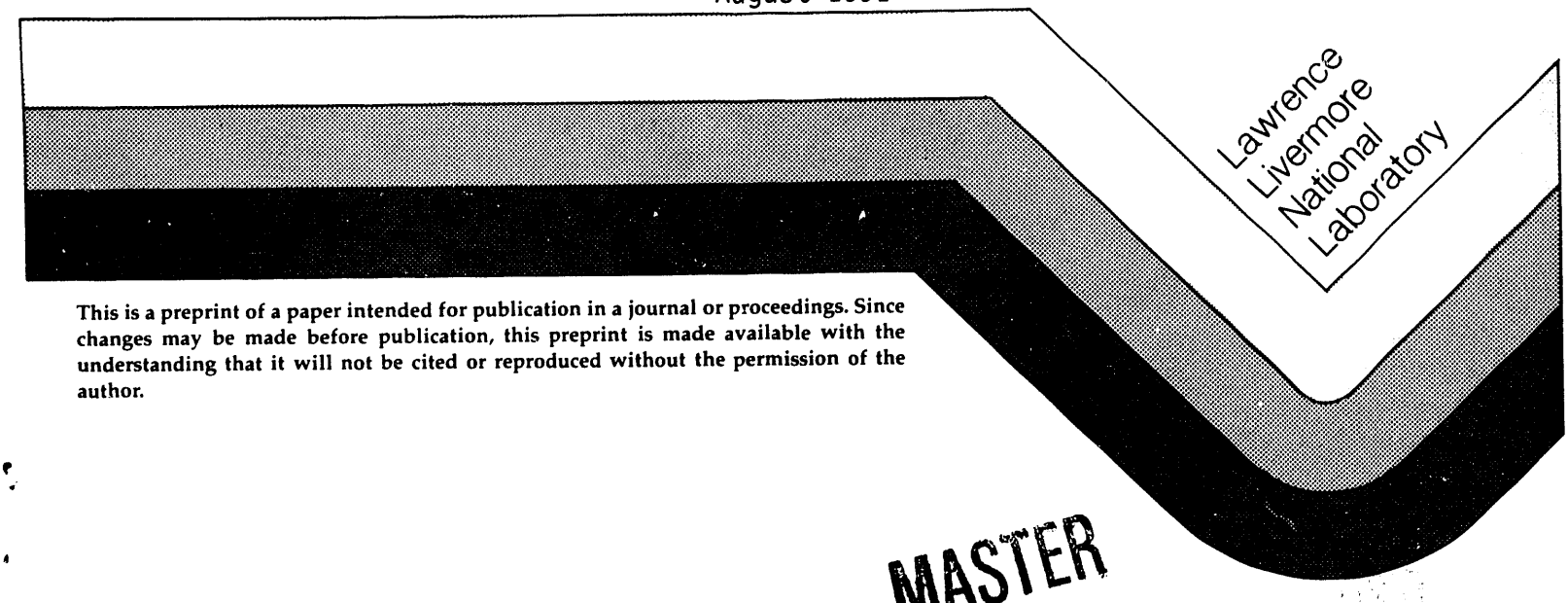

UCRL-JC--108161

DE92 002190

IMPACT OF THE ICE PHASE ON A MESOSCALE CONVECTIVE SYSTEM: IMPLICATION OF CLOUD PARAMETERIZATION AND CLOUD RADIATIVE PROPERTIES

Hung-Neng S. Chin, Michael M. Bradley, Charles R. Molenkamp
Keith E. Grant and Catherine Chuang

Lawrence Livermore National Laboratory
Livermore, California
U.S.A.

1. INTRODUCTION

Global climate change has been a continuous process for a long period of time. With the projected sea-level rise and influence on the water supply and agriculture, global warming has become a major issue of great scientific interest. According to observational and modeling results, increasing evidence shows that the upper-level cirrus anvil plays an important role on the large-scale climate through the cloud-radiation interaction. Climate prediction is, however, far from accurate due to a lot of uncertainties in the model physics. The largest of these is attributed to the inadequate understanding of the role of clouds in the climate system. This factor can affect the cloud amount and distribution and the interaction of clouds with solar and terrestrial radiation, and lead to an uncertainty of a factor of two in the amount of warming.

As indicated in earlier studies, the heating / cooling rate of longwave and shortwave radiation is primarily related to the vertical distribution of condensate in clouds. Thus, the transformation of cloud from the liquid phase to the ice phase can strongly impact the cloud radiative properties. Therefore, the significance of the ice phase on the large-scale climate can be recognized in two aspects. One is mainly related to the collective effects of cloud ensemble, such as cloud heating and drying effects. The other aspect is associated with the radiative properties of upper tropospheric cirrus / anvil clouds and their feedback on the large-scale climate.

Many modeling studies have shown that the results of large-scale models are very sensitive to the cloud heating profile (e.g., Anthes and Keyser, 1979). Thus, an interesting question is raised herein to address whether the heating profiles of cloud ensembles are sensitive to the types of condensate under consideration. In addition, the moisture transport property of cloud

ensembles has not been well studied in GCM (general circulation model) cloud parameterizations. The formation and maintenance of anvil clouds are, however, much related to this process. The further understanding of the impact of the ice phase on cloud ensemble features can help obtain a better parameterization for partitioning the condensed moisture into water and ice phases, and to improve the effect of cloud / radiation feedback in GCMs.

Some recent studies have attempted to investigate the perplexing effects of cloud feedback on global warming, based on the observed relationships between cloud water content and cloud temperature and on the dependence of cloud albedo and cloud emittance on cloud liquid water (Paltridge, 1980; Somerville and Remer, 1984). The systematic investigation of the dependence of cloud optical properties on explicit cloud information given by a dynamics-based cloud model has, however, not been well done in the literature. This is also one of the motivations of this study. The whole study is conducted by investigating the differences of the simulations with and without the ice phase in the microphysical process.

2. MODEL DESCRIPTION

For the computational efficiency, a two-dimensional cloud model is used to study a midlatitude squall line system of broken-line type, and to capture the dynamics of concern. The model is an extension of Chin and Ogura's (1989) two-dimensional model . The major differences are the inclusion of ice microphysics and radiation. The Coriolis force is neglected to render the model strictly two-dimensional. The model includes a planetary boundary layer (Blackadar, 1979) and uses a staggered grid. The surface temperature and vapor mixing ratio are fixed throughout the simulation in excess of 2 °C and 1 g kg^{-1} to the initial sounding at the lowest grid (i.e., 34 °C and 12.8 g kg^{-1}, respectively). Orlanski's (1976) open boundary condition is used at the lateral boundaries. The upper and lower boundaries are imposed by a rigid boundary condition . A sponge damping layer is placed above 15 km to minimize the reflection of internal gravity waves from the upper boundary. The grid resolution is stretched in the vertical and horizontal coordinates. The vertical grid is stretched ranging from 150 m near the surface to 600 m at 5.4 km high, and then becomes uniform up to 20.3 km. The horizontally uniform grid (2 km) is specified in the inner 600 km and then stretched outward from both sides of uniform grids with a stretching ratio of 1.15. The horizontal stretched grid is used to have a larger domain size (4640 km wide) to avoid possible influence from the lateral boundaries and to prevent the model convection from decay due to the limited moisture supply in a small model domain. The model grids are moved with the simulated squall line systems to keep the main features in the central portion of model domain at a speed of 17.0 and 17.5 m s^{-1} for ice-free and ice runs, respectively. The budget study

of heating (Q_1) and drying (Q_2) is based on Yanai *et al.*'s definition (1973) and the mass flux (M) is defined by $M = \rho g w$, where ρ is the density of air, g gravity and w vertical velocity.

2.1 Microphysics Parameterization

The model's microphysics includes warm and cold cloud processes. The warm cloud microphysics is based on Kessler's (1969) and Ogura and Takahashi's (1971) parameterizations, and contains two categories of condensates (i.e, cloud droplet and raindrop). In addition to these two types of condensates, ice crystals, snow and hail are also considered in the cold cloud process. The ice microphysics is based on Lin *et al.*'s (1983) parameterization with minor modifications to simulate a squall line system with a more prominent anvil (Fovell and Ogura, 1988). These modifications include the neglect of the Bergeron process and the accretion processes of ice crystals and snow by hail in the dry growth of hail. To prevent a significant amount of hail from reaching the ground, the hail intercept value is increased by a factor of 10 for the squall line system under consideration. The ice-free simulations adopt Soong and Ogura's (1973) moisture adjustment technique. This part is derived in a similar manner in the ice simulation so that the moisture field is adjusted in a way based on the mixture of cloud droplets and ice crystals. The mixing ratio of the mixed-phase cloud is given by the linear weighting parameters of δ and ε with respect to water and ice, respectively. As in Lord *et al.* (1984), the parameters δ and ε are taken to be the fraction of the pre-adjusted temperature T* within the range of (T_1, T_0), where $T_0 = 273$ K and $T_1 = 233$ K; δ is 1 as $T > T_0$ and ε equals 1 as $T < T_1$. The sum of these two parameters is unity at any grid point for any time.

In the ice microphysics, the evaporation of raindrops, sublimation of snow and hail, and deposition of snow are calculated with respect to the saturated mixed phase so that supersaturation is not allowed relative to the mixed phase after the moisture adjustment. Thus, it is not necessary to consider the deposition of snow in the ice simulation. Nonetheless, the adjusted moisture field might be supersaturated with respect to ice and subsaturated with respect to water for the mixed-phase cloud.

2.2 Radiation Parameterization

The radiation scheme implemented in the LLNL (Lawrence Livermore National Laboratory) chemical-transport model is used in this studies. The shortwave radiation scheme originally comes from Davies (1982), in which the Delta-Eddington approximation and adding-layer method are used to calculate the scattering from the direct beam and to treat multiple scattering between layers. The longwave radiation scheme is basically developed by Harshvardhan and Corsetti (1974). A

further modification is made to distinguish the radiative properties of ice cloud from those of water cloud for shortwave (SR) and longwave radiation (LR), using the radiation parameterization schemes of Stephens (1978) and Starr and Cox (1985) for water and ice clouds, respectively. The mixed-phase cloud is also considered. Cloud optical properties are functions of predicted condensates which are, in turn, temperature dependent in the microphysical process. Hence, the temperature field is the major factor to determine the radiative properties of clouds.

The top of the model domain used for calculating radiation fluxes is extended to 1 mb by adding 5 more layers above the cloud model domain. The surface albedo is specified as 0.2. The CO_2 concentration is assumed well-mixed within the whole atmosphere at 320 ppm. The mixing ratio of O_3 is given by climatological data from McClatchey *et al.* (1972). The moisture and temperature profiles for radiation calculation above sounding levels (150 mb) are also based on climatological data. The effect of aerosol on the radiation is not considered in this study.

3. INITIALIZATION

The initial conditions are based on a composite squall line sounding for broken-line type systems (Bluestein and Jain, 1985) with the temperature and moisture profiles modified to represent a mixed layer below 800 mb, as is often observed in the pre-storm condition in midlatitudes (Fig. 1). The broken-line system is the predominant type of convection in Oklahoma springtime severe storms, and is chosen herein as a representative of mid-latitude convection. Due to the small helicity (Lilly, 1983) of broken-line systems, the base state wind (normal to the squall line) with unidirectional shear is used (Fig. 2). The vertical wind shear below 5 km is approximately constant at 4 m s^{-1} per 100 mb. A constant wind is imposed above 5 km for simplicity. The CAPE (convective available potential energy) value and bulk Richardson number of the initial conditions are 2216 J kg^{-1} and 56, respectively. The lifting index of this modified sounding is -7.8 °C.

The model is initialized with a warm, moist bubble and a horizontally homogeneous sounding. This bubble is 10 km wide and 2 km deep, and is centered at 1.9 km above the ground. The maximum perturbations of potential temperature and moisture are 2 K and 4 g kg^{-1}, respectively.

4. RESULTS

None of the model results shown include radiation effects. The radiation model is only used to diagnose the cloud radiative properties in the following context, based on the cloud model outputs. The simulation with higher horizontal resolution (1 km) is also performed to test the

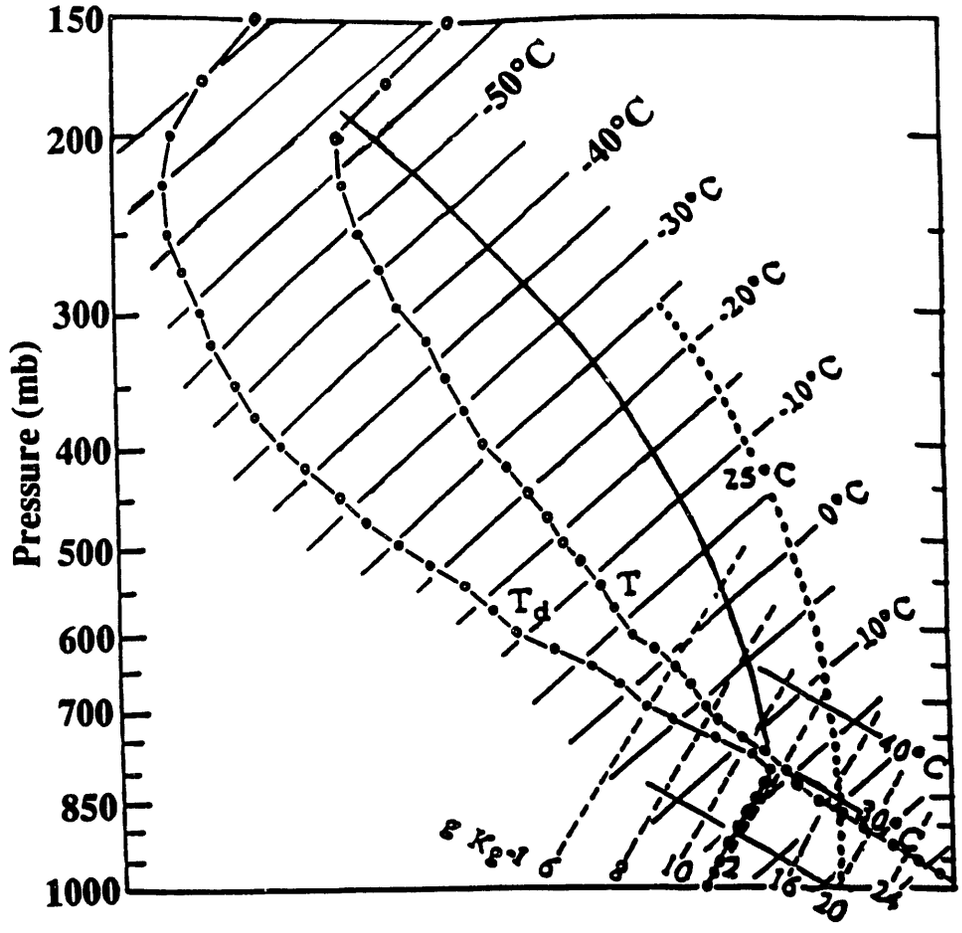

Fig. 1. The modified atmospheric sounding for the broken-line type of squall line system.

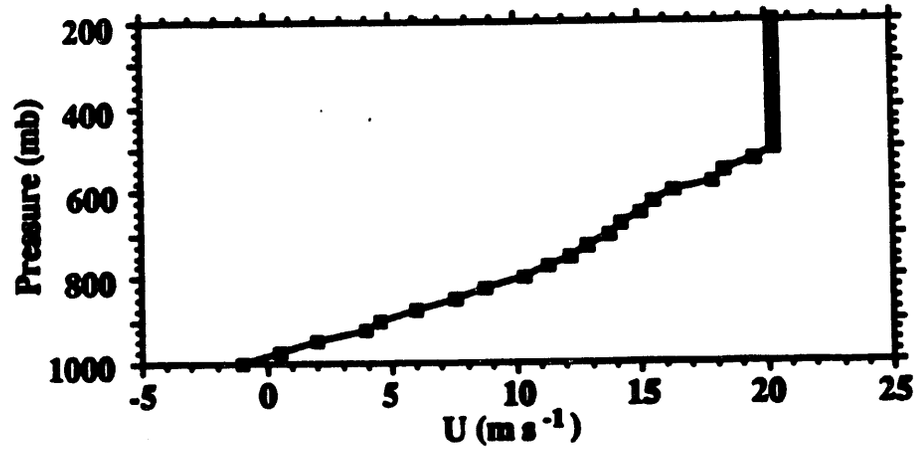

Fig. 2. The base state wind (normal-line component) profile used in this study.

sensitivity of model solutions. Results indicate that the general characteristics of model solutions are insensitive to the horizontal resolution under consideration. Nonetheless, the experiment with finer resolution predicts a more intense system that evolves faster. Therefore, only the results with 2-km resolution are shown in this study.

The evolution of induced maximum vertical velocity and surface potential temperature deviation of the ice-free run is shown in Fig. 3. The results show that the initial convections repeat the life cycle and grow in the first 3 hours, then model solutions are set up into two stable modes, marked as A and B in Fig. 3. The most striking differences of these two modes are found in the intensity and tilting of convective core. The transition of stronger mode (A) to weaker one (B) coincides with the occurrence of maximum cold pool intensity. This feature is consistent with Rotunno *et al.*'s (1988) finding. The dominant cold pool tends to tilt the convection to the upshear side and leads to a less-than-optimum situation for a long-lived squall line. Up to the time that the convection is terminated, the predicted system is still in the quasi-steady state and does not show any sign of decay. Based on the distinct evolution character of the predicted system, the whole evolution is divided into three stages; initial, developing and mature stages. The developing stage is characterized by the nearly up-right tilting of the convective core and the mature stage is unique in its upshear tilting. Only the developing and mature stages are chosen to show their quasi-steady features in the cloud ensemble properties.

The time-distance cross-section of the surface precipitation rate of both the ice-free and ice runs are depicted in Fig. 4. In general, two distinct modes are captured in both runs. One is characterized by the well-defined repeated cycle (stationary in the domain-relative frame) before 6 hours. The other is distinguished by the faster propagation of the leading edge and the far separation of dominant convection from the leading edge, defined by the -1 K isotherm of surface potential temperature anomaly. In the mature stages (6-9 hours) of both runs, the convective core tilts upshear and the decayed convective cell is towed to the upshear side so that the surface precipitation of individual convection tends to move westward (upshear) with time although the whole system still propagates eastward (downshear). This feature is particularly clear in the ice run due to its stronger intensity.

4.1 Validation of model solutions

The hourly-mean dynamic structure of the ice-free run during the end of mature stage is illustrated in Fig. 5. The ice run (not shown) has a similar structure. The general patterns of induced vertical motion and horizontal velocity (relative to the system) bears a strong similarity to the observed features of a broken-line squall system (e.g., Ogura and Liou, 1980). These features include upshear tilting of the convective core, decayed convection located at the upshear side of

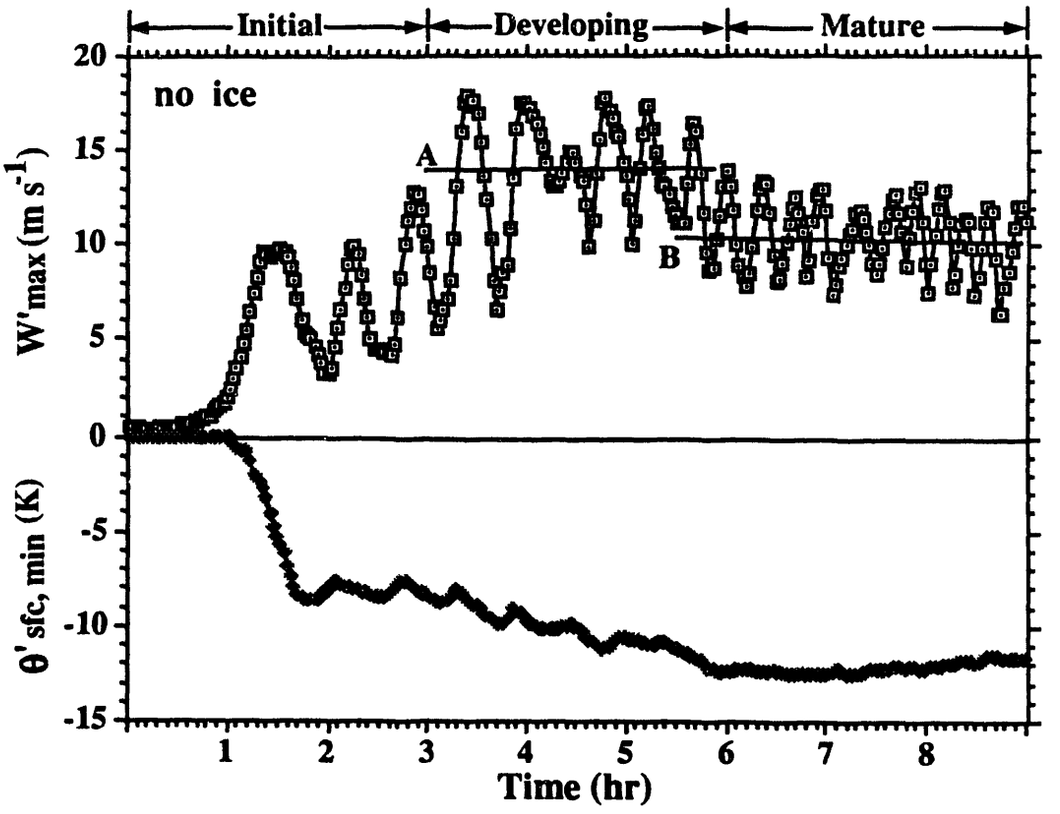

Fig. 3. Time history of domain maximum vertical velocity (m s^{-1}) and surface minimum potential temperature anomaly (K) of ice-free run.

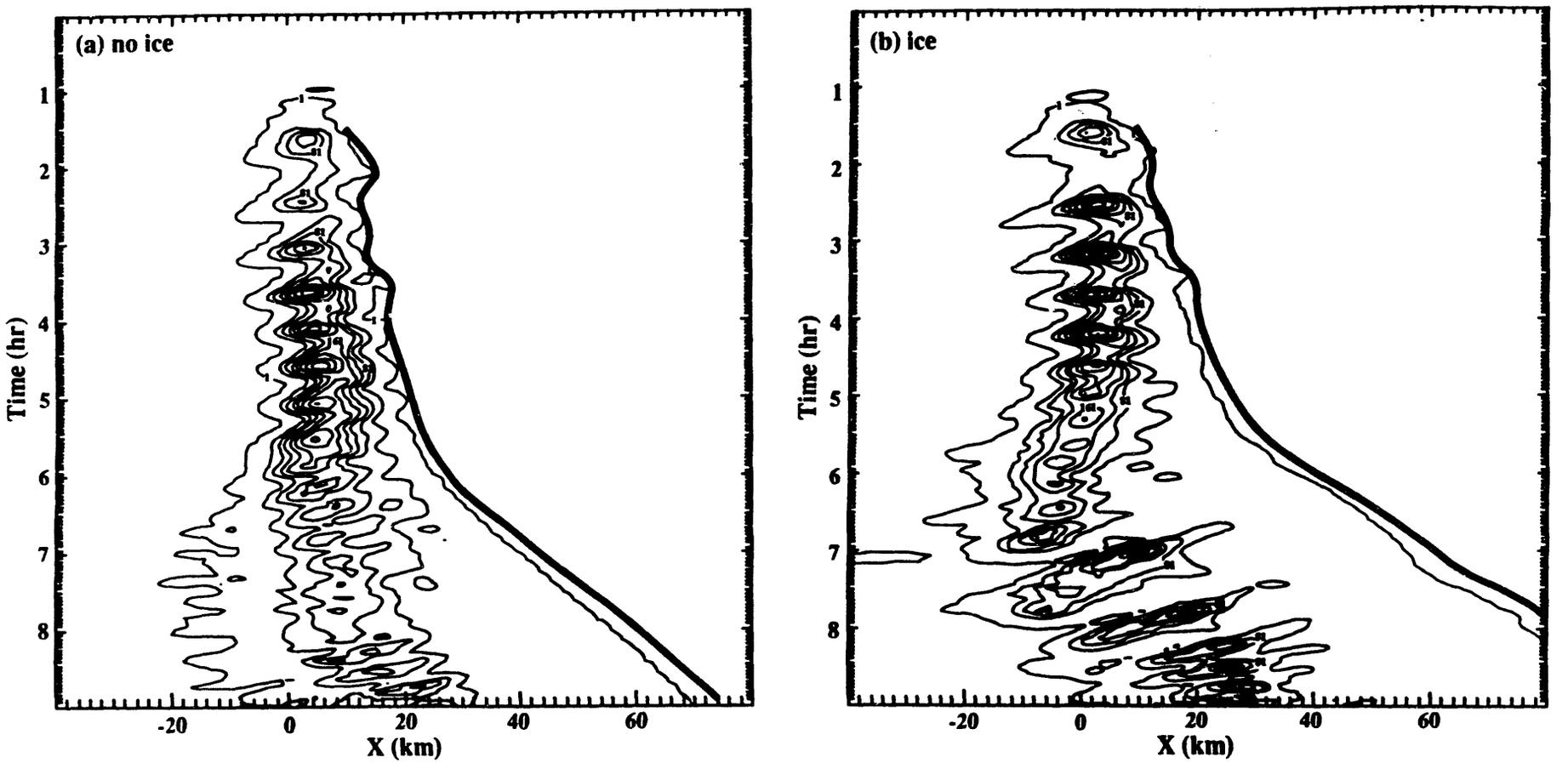

Fig. 4. Time-distance cross-section of surface precipitation rate. Intensities are shown with a interval of 40 mm hr^{-1}, starting from 1 mm hr^{-1} in the domain-relative frame. The thick line represents the leading edge, defined as -1 K of surface potential temperature anomaly. (a) ice-free run. (b) ice run.

developed deep convection, strong easterly flow prevailing in the region of upward motion, upper-level downshear westerly outflow, rear low-level inflow (westerly) and rear outflow underneath. The dynamic structure of vertical velocity, horizontal wind, potential temperature and moisture anomalies shown in Fig. 5 also bears a strong similarity to Fovell and Ogura's (1988) modeling study for the same type of squall line system.

A comparison of predicted time- and domain-averaged heating (Q_1) and drying (Q_2) effects of the ice run with the observed data of the same type of squall line system (Gallus and Johnson, 1991) at the mature stage is shown in Fig. 6. The time span is during the last hour (8-9 h) of the ice run and the horizontal size of the subdomain is chosen to be the same as the one in the observational study (i.e., 200 km). Note that the surface layer of the observed data is located at 950 mb, and the model surface is at 1000 mb. In general, the predicted heating profile is in a good agreement with observed features, such as the upper-level (6-9 km) twin peaks and low-level (3-4 km) weaker local heating maximum. The unique upper-level twin peaks of heating profile are caused by the heat flux transport, particularly in the stratiform-cloud region (Fig. 7a and c). In contrast, the dominant upper-level peak of observed drying effect is in sharp contrast to the predicted Q_2 profile and many others of different convective systems. Another observational evidence of broken-line squall system, however, supports the predicted distribution (Ogura, and Chen, 1977). The predicted low-level dominant peak of the Q_2 profile is explained by the adding effect of net condensation and moisture flux transport by cloud-scale motion in the lower levels and the canceling effect of both in the upper levels (Fig. 7d and e). Similar patterns of heating and dry effects are also captured in the ice-free run (not shown).

4.2 Heat, moisture and mass flux budgets of cloud ensemble

The comparisons of time-horizontally averaged heating and drying effects and mass flux of ice-free and ice runs at developing and mature stages are depicted in Fig. 8. The time span and horizontal size of subdomain are 3 hours and 200 km, respectively. The general patterns of heat, moisture, and mass flux profiles are in a good agreement between the ice-free and ice runs, except for the finer structure in the heating and drying profiles of the ice run and the surface layer features. Simulations without surface heat and moisture fluxes from the planetary boundary layer were also performed for comparison (not shown). The general solutions without the planetary boundary layer remains about the same as the one with it. The only difference is attributed to the heat and moisture budgets near the surface layer. These results suggest that the planetary boundary layer physics has little dynamic influence on the squall line system, but it does make a contribution to the surface heat and moisture budgets, particularly in the heating budget to balance the strong evaporative cooling of rain water (about -7 °C during the last hour of ice run).

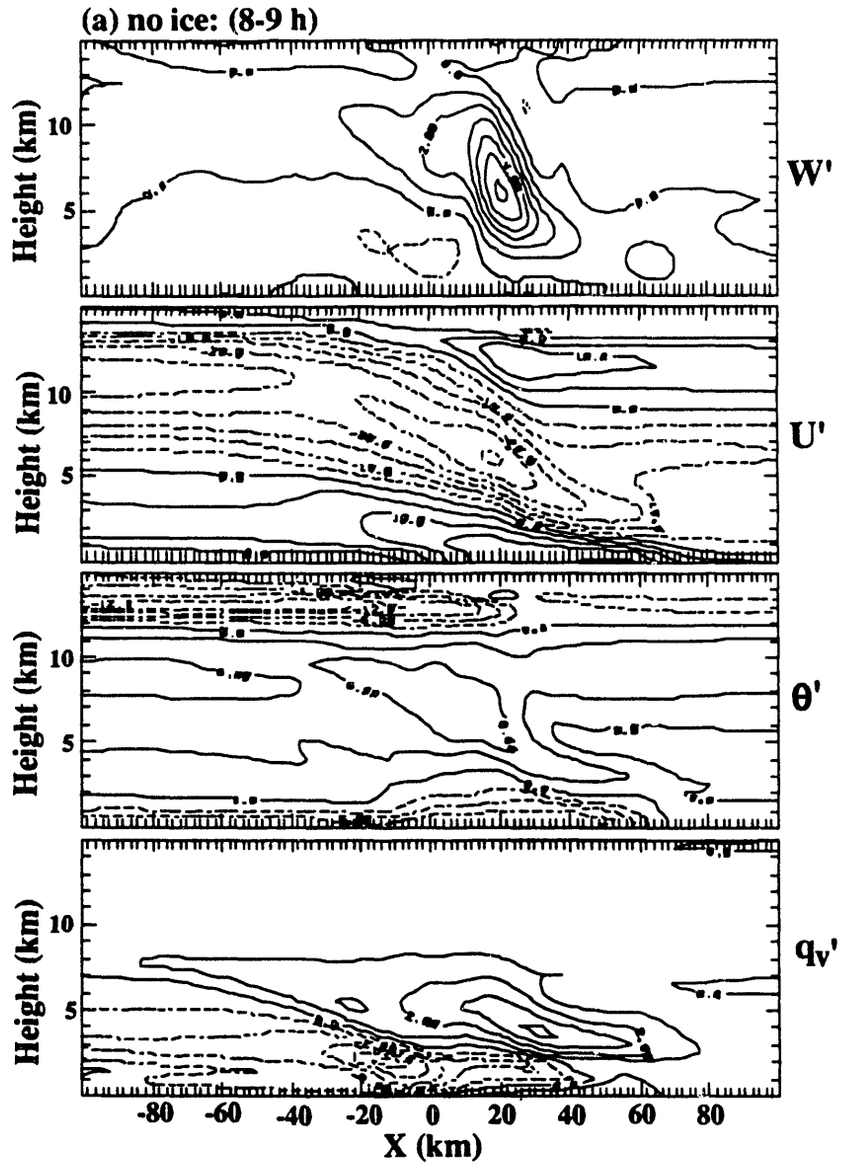

Fig. 5. Time-averaged cross-sections of ice-free run. (a) induced vertical velocity with contour of 1 m s^{-1}. (b) induced relative horizontal velocity with contour of 5 m s^{-1}. (c) potential temperatue deviation from base state with contour of 3 K. (d) moisture deviation from base state with contour of 1 g kg^{-1}.

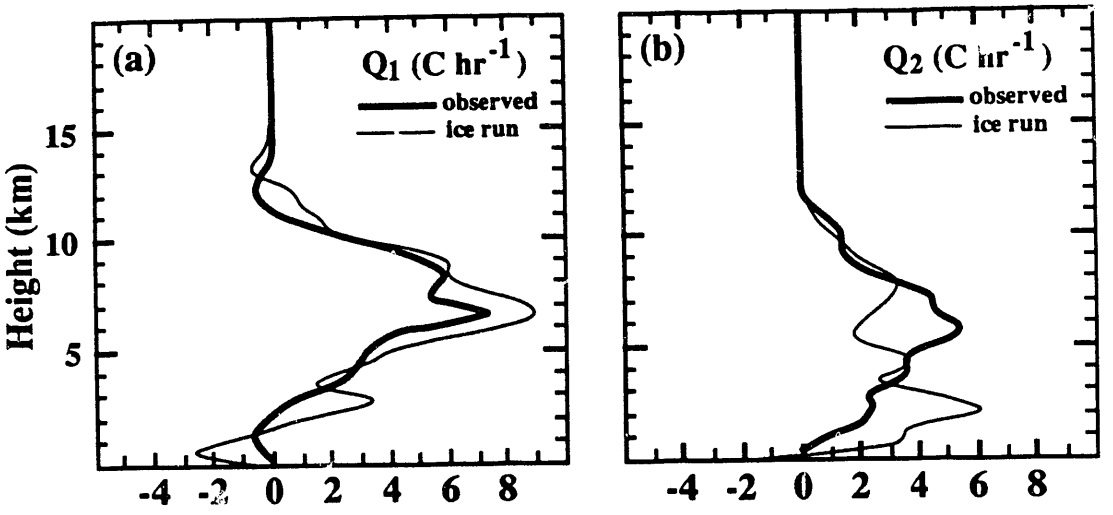

Fig. 6. Time-horizontally averaged profiles of ice run during 8-9 hours. (a) heating effect (Q_1). (b) drying effect (Q_2).

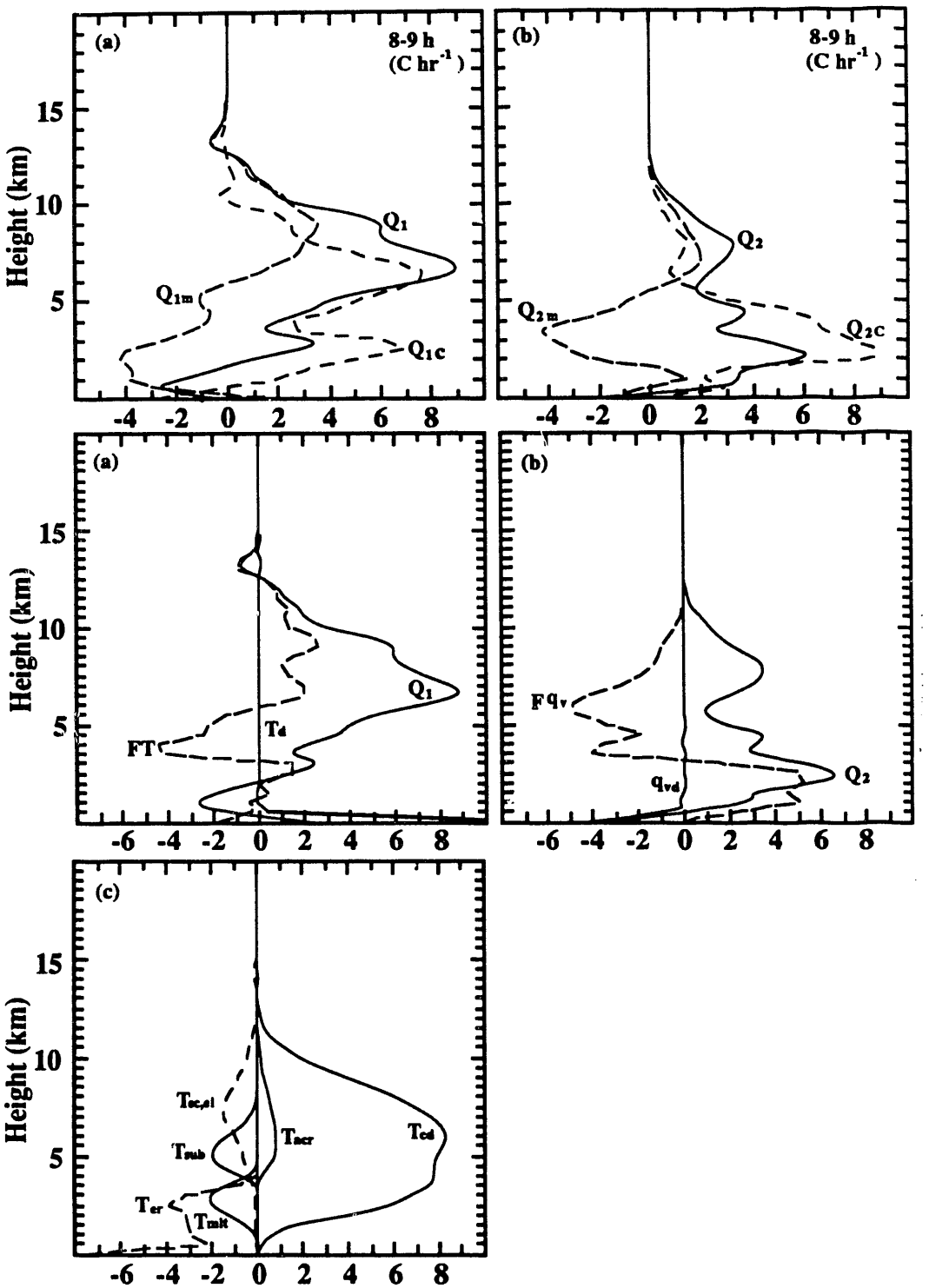

Fig. 7. Time-horizontally averaged profiles of ice run. FT and Fqv are net vertical fluxes of sensible heat and moisture by clouds. T_d, T_{er} and T_{cd} are temperature changes due to turbulence, evaporation of raindrops and condensation. T_{mlt}, T_{sub}, T_{acr} and $T_{ec,\,ei}$ are temperature changes due to melting and sublimation of snow and hail, accretion process and evaporation of cloud droplet and ice crystal.

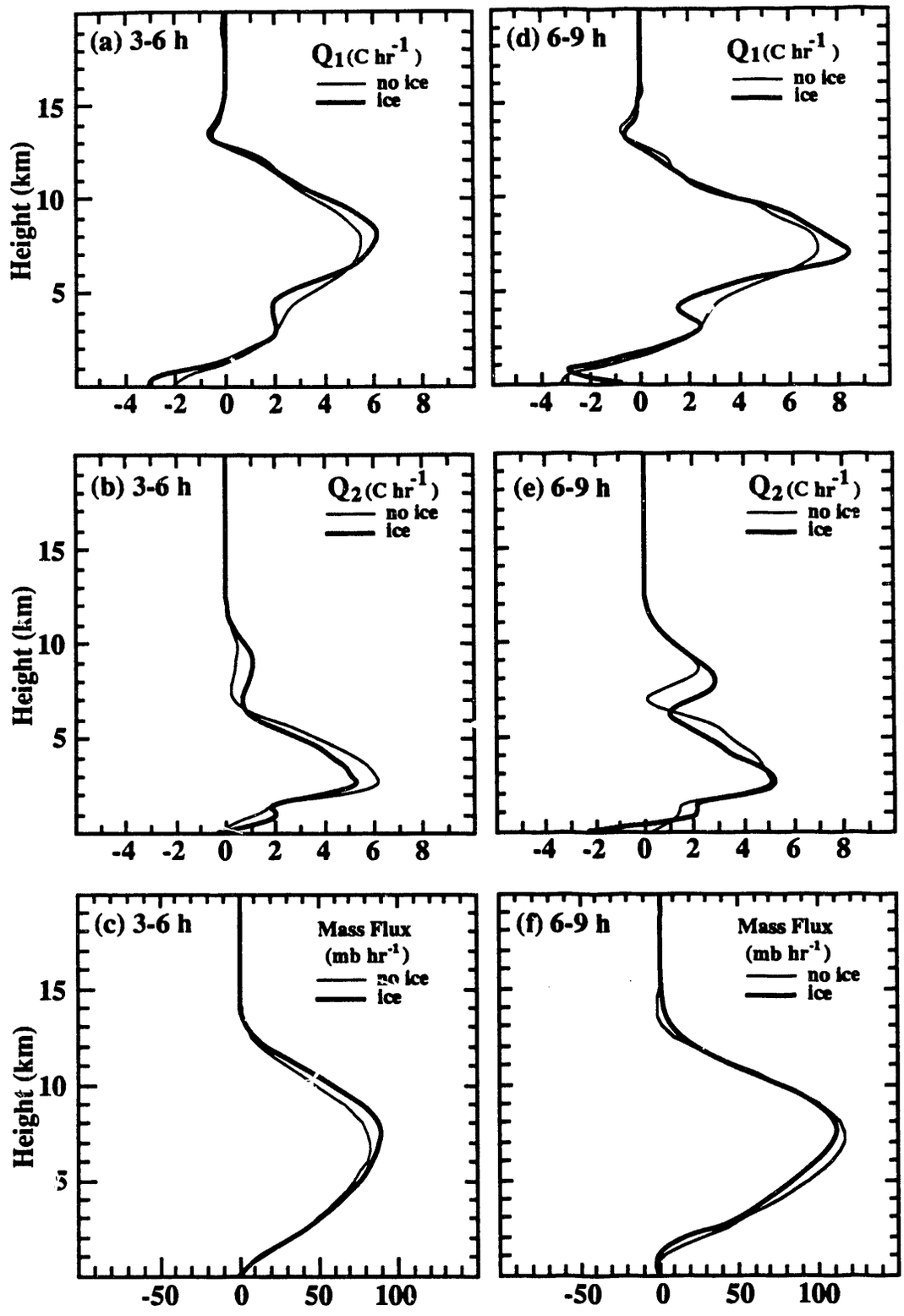

Fig. 8. Time-horizontally averaged profiles of ice-free and ice runs at developing and mature stages. (a), (d) heating effect (Q_1). (b), (e) drying effect (Q_2). (c), (f) mass flux.

The finer structure of heating profiles in the ice run is attributed to the stronger condensation at upper levels and the more intense heat flux cooling at lower levels (Fig. 9). The total heating effect (vertical integration), however, remains about the same between both runs (Fig. 10). A similar conclusion is also found in the drying effect (Fig. 10). The relatively large difference on the total heating and drying effects at the mature stage is mainly caused by the contrast near the surface layer. Above the surface layer, these differences are negligibly small.

The water budget of the simulated squall line system is discussed in this section. Owing to the usage of a moving grid system, the total water mass (including moisture and all types of condensates) conservation can not be assessed in the subdomain, since a large portion of moisture is depleted by the microphysical process and left behind the area of concern. An alternative way to assess the water budget is evaluated in terms of the total storage of condensates (S), total precipitation fall-out (P) and net outflow of total condensates (A) through the lateral boundaries of subdomain.

Once the microphysical processes take place, the condensed moisture can be transformed into different types of condensates. Most of that falls out as precipitation and some is carried into upper levels and moved away through the lateral boundaries of the subdomain by the upper-level outflow. The rest remains in the subdomain as the storage term. Thus, the net total condensed moisture (M) within the subdomain of concern can be expressed by $M = S + P + A$. The revised water budgets of the ice-free and ice runs at developing and mature stages are listed in Fig. 11. Both simulations show a consensus in the contribution of storage, outflow and fall-out terms relative to the condensed moisture. The storage rate (S/M) decreases from developing to mature stage. Conversely, the outflow (A/M) and fall-out rates (P/M) increase as the solution evolves from the developing to mature stage. An efficient fall-out rate (over 90 %) is found in all situations. The outflow term (A), mainly contributed by the anvil outflow, is the only process to interact with the neighboring environment. This term is particularly small in the developing stage. As the system keeps growing, the outflow term becomes as important as the storage term.

For general application in GCM cloud parameterization, the storage term can be redistributed into water and ice phase, relying on the temperature dependence. Therefore, the microphysical condensates could be represented without using prognostic equations to save computer time and to simplify the model physics. The radiative properties of condensates are, however, captured in the model without much effort. As to the outflow term, it can be equally separated to interact with neighboring columns for simplicity.

4.3 Radiative properties of anvil clouds

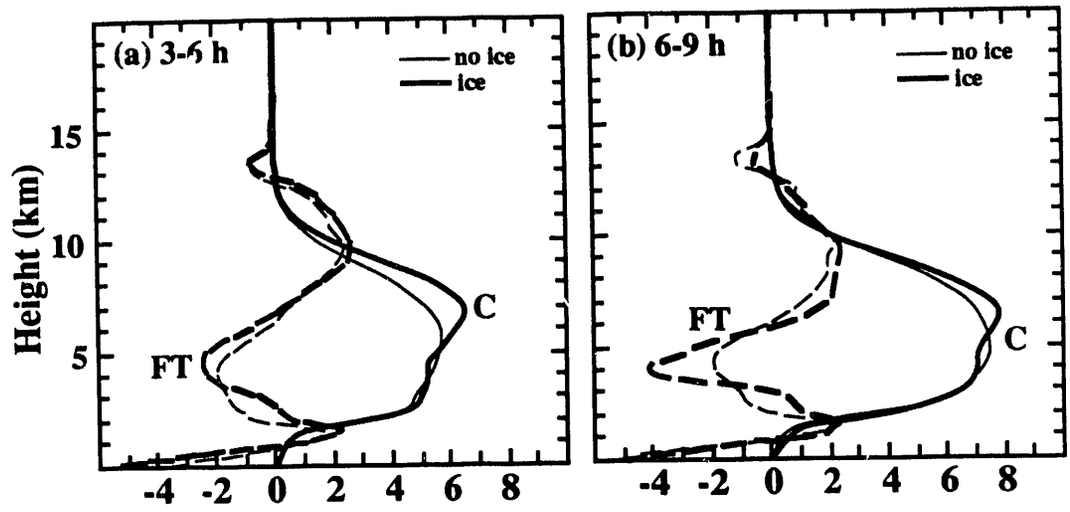

Fig. 9. Heating profiles of condecsation (C) and heat flux transport by clouds (FT) at developing and mature stages for ice-free and ice runs.

Unit: C hr^{-1}

no ice	3-6 h	6-9 h
$\sum_{z_1=1}^{20} Q_1$	67.2	72.6
$\sum_{z_1=1}^{20} Q_2$	47.3	52.1

ice	3-6 h	6-9 h
$\sum_{z_1=1}^{20} Q_1$	67.0	74.6
$\sum_{z_1=1}^{20} Q_2$	46.9	54.8

Fig. 10. Total heating and drying effects of ice-free and ice runs at developing and mature stages.

Unit: x 10^9Kg

no ice	3-6 h	6-9 h
S	0.54	0.06
A	0.03	0.07
P	5.84	7.10
M	6.41	7.23
$\frac{S}{M}$	8.4%	0.8%
$\frac{A}{M}$	0.5%	1.0%
$\frac{P}{M}$	91.1%	98.2%

ice	3-6 h	6-9 h
S	0.50	0.37
A	0.18	0.33
P	6.14	8.05
M	6.82	8.75
$\frac{S}{M}$	7.3%	4.2%
$\frac{A}{M}$	2.6%	3.8%
$\frac{P}{M}$	90.0%	92.0%

Fig. 11. Water budgets of ice-free and ice runs at developing and mature stages.

The time-averaged temperature, moisture and condensate distributions at the developing stage of both the ice-free and ice runs are used to diagnose the radiative properties of water and ice anvils. The time-averaged cloud structure (Fig. 12) indicates that a prominent anvil located near 12 km exists in both runs. The total mass of condensate (including cloud droplet, ice crystals and snow) in the ice anvil is about four times its counterpart (cloud droplet only) in the water anvil. In addition to the intensity, the significant differences between these two runs have to do with the horizontal and vertical extent of the anvil cloud. The time-horizontally averaged (200 km) heating profiles of longwave (LR), shortwave radiation (SR) and the net radiation (NET) are shown in Fig. 13. The shortwave radiation is calculated at noon as an upper bound for comparison with the longwave radiation, although the broken-line squall systems usually occurred in the late afternoon or evening. In general, heating profiles of LR for both runs exhibit similar features, such as the heating near the bottom of the anvil cloud and the cooling near the cloud top. The thicker ice anvil has a larger heating/cooling contrast throughout the anvil cloud than the water anvil. Even though the magnitude of LR heating and cooling is much less than the cloud heating effect, this temperature destabilization is favorable to create local instability for intensifying the anvil cloud, particularly in the ice anvil.

In contrast, the ice phase has a more significant impact on the shortwave radiation. The optically thick water anvil absorbs most of the solar radiation in a short physical distance and leads to a rather strong heating near the cloud top. The translucent feature of the ice anvil, however, allows the solar radiation to penetrate for a longer distance, and to form a rather weak heating peak near the middle of ice anvil. The net radiative effect in the water anvil tends to develop multi-layer structure, which seems to be unfavorable for the maintenance and persistence of upper-level anvil.

5. SUMMARY

This study attempts to provide further understanding of the effect of the ice phase on cloud ensemble features which are useful for improving GCM cumulus parameterization. In addition, cloud model results are used to diagnose the radiative properties of anvils in order to assess cloud / radiation interaction and its feedback on the larger-scale climate for the future work. The heat, moisture and mass budget analyses of a simulated squall line system indicate that, at least for this type of system, the inclusion of the ice phase in the microphysics does not considerably change the net cloud heating and drying effects and the feedback on the large-scale motion. Nonetheless, its impact on the radiative properties of clouds significantly influences not only the squall line system itself, but also the larger-scale circulation due to the favorable stratification for long-lasting anvil clouds.

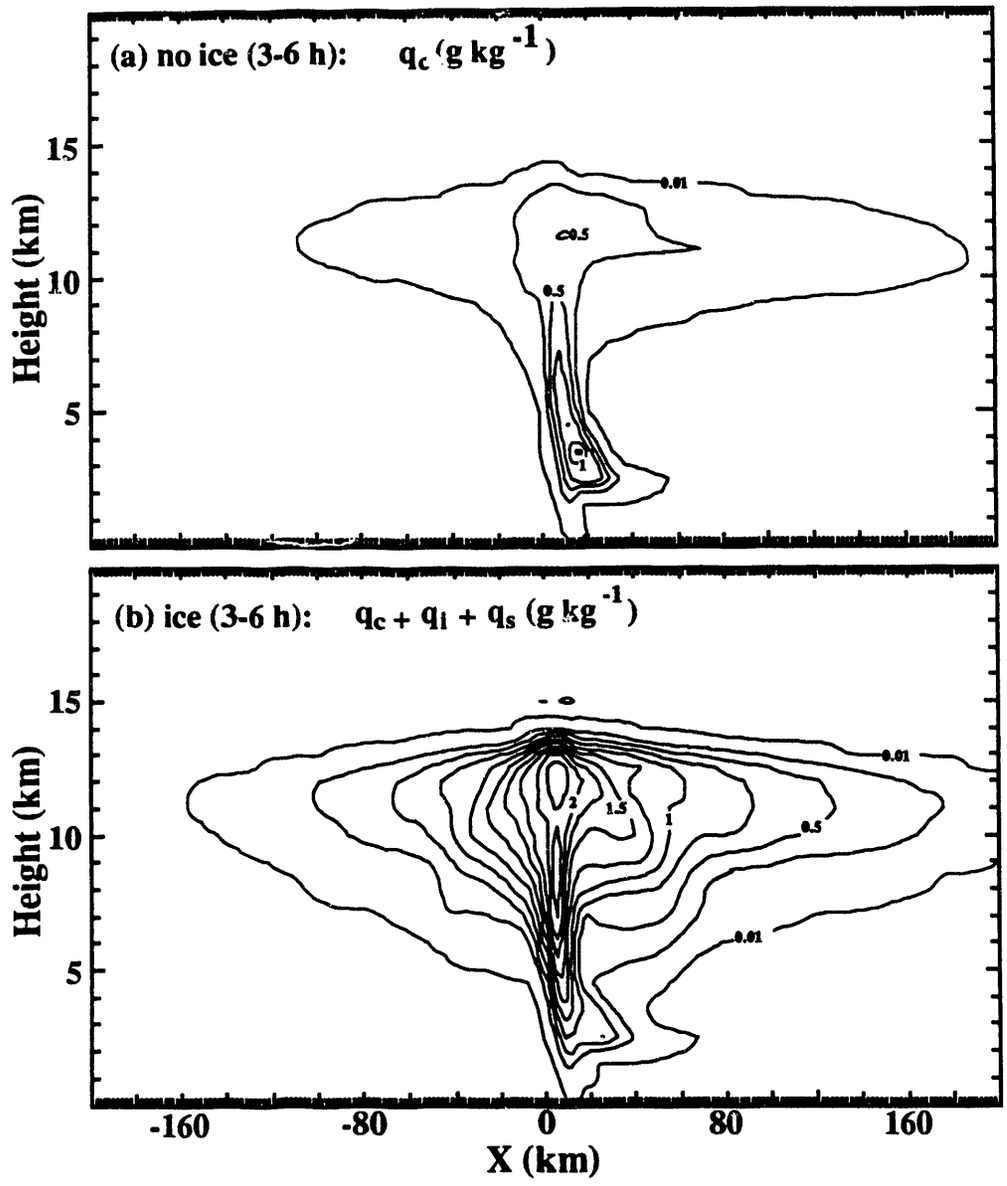

Fig. 12. Time-averaged cross-sections. Contours start with 0.01 g kg^{-1} and have intervals of 0.25 g kg^{-1}. (a) cloud water mixing ratio of ice-free run. (b) sum of cloud water, ice crystal and snow mixing ratio of ice run.

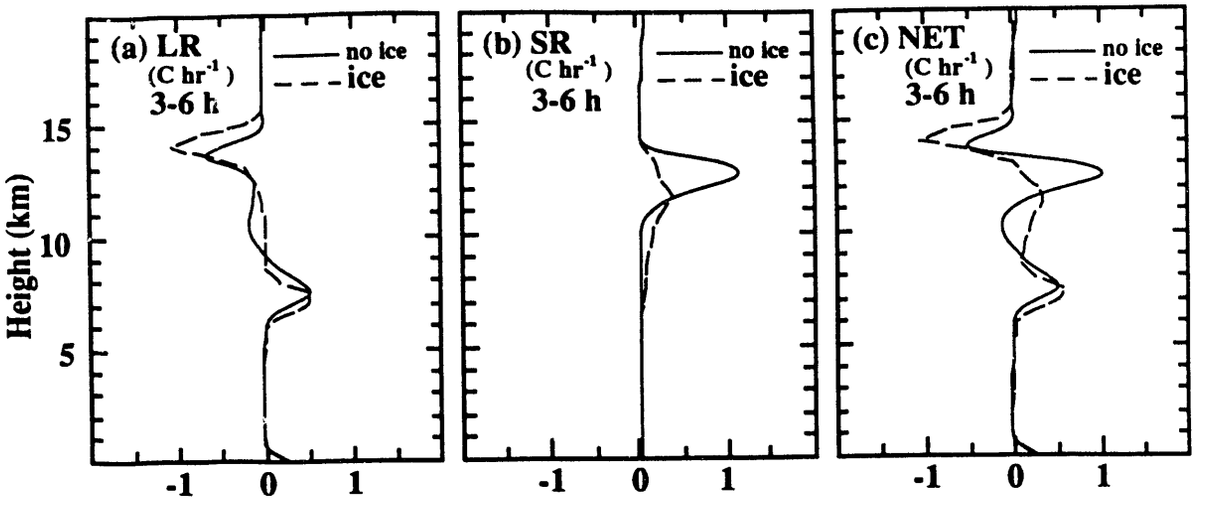

Fig. 13. Time-horizontally averaged heating rate of ice-free and ice runs at the develping stage in unit of C hr^{-1}. (a) longwave radiation (LR). (b) shortwave radiation (SR). (c) net radiation.

The water budget suggests a simple methodology to parameterize the microphysical effect without considering it as a model physics module. Further application of the water budget might also be used to parameterize the cloud transport of condensates in the anvil cloud region, which allows the GCM columns to interact with each other. The findings of this study suggest that the ice phase could be ignored in the cloud parameterization in order to save significant amounts of computational resources and to simplify the model physics. More scientific effort should, however, be focused on the effect of the ice phase to further explore cloud feedback on the large-scale climate through the radiative process. The cloud / radiation interaction and its feedback on the larger-scale climate will be addressed in a companion study by coupling the radiative transfer model with the cloud model.

6. ACKNOWLEDGEMENTS

The authors wish to express their appreciation to Dr. Robert G. Fovell for sharing his ice parameterization scheme. This work was supported by the Institutional Collaborative Research (INCOR) program and conducted under the auspices of the U.S. Department of Energy by the Lawrence Livermore National Laboratory under Contract W-7405-Eng-48.

7. REFERENCES

Anthes, R. A., and D. Keyser, 1979: Tests of a fine-mesh model over Europe and the United State. Mon. Wea. Rev., 107, 963-984.

Blackadar, A. K., 1979: High resolution models of the planetary boundary layer. Advances in environmental and science engineering, Vol. 1, J. R. Pfafflin and E. N. Ziegler, Eds., Gordon and Breach, 276 pp.

Bluestein, H. B., and M. H. Jain, 1985: Formation of mesoscale lines of precipitation: Severe squall lines in Oklahoma during the spring. J. Atmos. Sci., 42, 1711-1732.

Chin, H.-N. S., and Y. Ogura: Supplementary modeling study of a tropical convective band. J. Atmos. Sci., 46, 1440-1447.

Davies, R.: Documentation of the Solar radiation parameterization in the GLAS Climate Model, NASA Tech. Memo. 83961, Greenbelt Space Flight Cent., Greenbelt, Md., 57 pp, 1982.

Fovell, R. G., and Y. Ogura, 1988: Numerical simulation of a midlatitude squall line in two dimensions. J. Atmos. Sci., 45, 3846-3879.

Gallus, W. A. Jr., and R. H. Johnson, 1991: Heat and moisture budget of an intense midlatitude squall line. J. Atmos. Sci., 48, 122-146.

Harshvardhan, and T. G. Corsetti, 1984: Longwave radiation for the UCLA/GLAS GCM, NASA Tech. Memo. 86072, Greenbelt Space Flight Cent., Greenbelt, Md., 51 pp, 1984.

Lilly, D. K., 1983: Helicity as stabilizing effect on rotating convective storms. Preprints, 13th Conf. on severe local storms, Tulsa, Amer. Meteor. Soc., 219-222.

Lin, Y.-L., R. D. Farley, and H. D. Orville, 1983: Bulk parameterization of the snow field in a cloud model. J. Clim. Appl. Meteor., 22, 1065-1092.

Lord, S. J., H. E. Willoughby, and J. M. Piotrowicz, 1984: Role of a parameterized ice-phase microphysics in an axisymmetric, nonhydrostatic tropical cyclone model. J. Atmos. Sci., 41, 2836-2848.

McClatchey, R. A., R. W. Fenn, J. E. A. Selby, F. E. Volz, and J. S. Garing, 1972: Optical properties of the Atmosphere. AFCRL-72-0497, Air Force Cambridge Research Laboratory, L. G. Hanscom Field, Ma., 108 pp, 1972.

Ogura, Y., and M.-T. Liou, 1980: The structure of a midlatitude squall line: A case study. J. Atmos. Sci., 37, 553-567.

Orlanski, I., 1976: A simple boundary condition for unbounded hyperbolic flows. J. Comput. Phys., 21, 251-269.

Paltridge, G. W., 1980: Cloud-radiation feedback to climate. Quart. J. Roy. Meteor. Soc., 106, 895-899.

Somerville, R. C. J., and L. A Remer, 1984: Cloud optical thickness feedbacks in the CO2 climate problem. J. Geophys. Res. 89, 9668-9672.

Soong, S.-T., and Y. Ogura, 1973: A Comparison between Axisymmetric and Slab symmetric cumulus cloud models. J. Atmos. Sci., 30, 879-893.

Starr, D. O'C., and S. K. Cox, 1985: Cirrus clouds. Part II: Numerical experiments on the formation and maintenance of cirrus. J. Atmos. Sci., 42, 2682-2694.

Stephens, G. L., 1978: Radiation profiles in extended water clouds. II: Parameterization schemes. J. Atmos. Sci., 35, 2123,2132.

END

DATE FILMED

12/19/91